This is a repository copy of *Control of magnetic properties of liquid-crystalline dendron-modified FePt nanoparticles through thermal phase transition for tunable magnetic materials*.

White Rose Research Online URL for this paper:
https://eprints.whiterose.ac.uk/230155/

Version: Published Version

Article:
Yachi, T. orcid.org/0000-0001-5301-6231, Sato, R. orcid.org/0009-0002-9765-2533, Matsubara, M. et al. (6 more authors) (2025) Control of magnetic properties of liquid-crystalline dendron-modified FePt nanoparticles through thermal phase transition for tunable magnetic materials. ACS Applied Nano Materials. ISSN 2574-0970

https://doi.org/10.1021/acsanm.5c02325

Reuse
This article is distributed under the terms of the Creative Commons Attribution-NonCommercial-NoDerivs (CC BY-NC-ND) licence. This licence only allows you to download this work and share it with others as long as you credit the authors, but you can't change the article in any way or use it commercially. More information and the full terms of the licence here: https://creativecommons.org/licenses/

Takedown
If you consider content in White Rose Research Online to be in breach of UK law, please notify us by emailing eprints@whiterose.ac.uk including the URL of the record and the reason for the withdrawal request.

eprints@whiterose.ac.uk
https://eprints.whiterose.ac.uk/

ACS APPLIED NANO MATERIALS

Open Access
This article is licensed under CC-BY-NC-ND 4.0

www.acsanm.org
Article

Control of Magnetic Properties of Liquid-Crystalline Dendron-Modified FePt Nanoparticles through Thermal Phase Transition for Tunable Magnetic Materials

Takehiro Yachi, Rina Sato, Masaki Matsubara, Chen Shen, Rie Umetsu, Xiangbing Zeng, Goran Ungar,* Atsushi Muramatsu, and Kiyoshi Kanie*

Cite This: https://doi.org/10.1021/acsanm.5c02325

Read Online

ACCESS | Metrics & More | Article Recommendations | Supporting Information

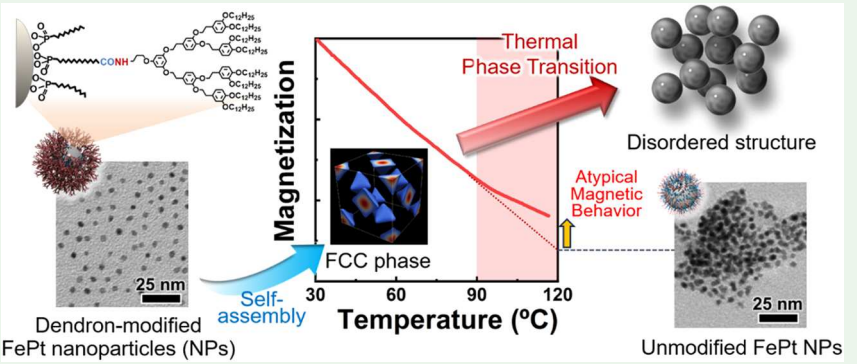

ABSTRACT: FePt nanoparticles (NPs) with thermally responsive array structures were prepared by surface modification with a liquid-crystalline phenylethyl ether-type dendron. Dendron modification was carried out in two steps. In the first step, COOH moieties were introduced on the surface of oleyl-modified FePt NPs by ligand exchange using terminal COOH-substituted *n*-alkyl phosphonic acid. This was followed by the amidation reaction between COOH moieties and the amino-substituted dendron. Infrared spectroscopic measurement and thermogravimetric analysis confirmed that the dendrons were successfully grafted onto the surface of FePt NPs. Transmission electron microscopy also showed an increase in interparticle distance due to dendron modification. Small-angle X-ray scattering (SAXS) revealed that the dendronized NPs pack on an FCC lattice, which melts above 100 °C in thermal response, consistent with the endothermic peak observed in differential scanning calorimetry (DSC). Electron density maps offer detailed insights into the structural organization of the dendronized FePt NP array. These results indicate that the formation of an FCC phase through self-assembly and its thermal transition into a disordered phase enabled dynamic control over magnetic NP arrays. Finally, changes in magnetic properties during thermal phase transition were investigated by a superconducting quantum interference device. The results show certain changes in magnetization behavior introduced by the thermal phase transition. These results demonstrate that dendron modification of FePt NPs enables the introduction of thermal responsiveness in their supramolecular structure and magnetic behavior. The flexible control of magnetic properties is expected to expand the application potential of the magnetic NPs used as building blocks for tunable smart magnetic devices.

KEYWORDS: *FePt nanoparticles, self-assembly, liquid crystal, dendrimer, organic−inorganic hybrid materials*

INTRODUCTION

Magnetic nanoparticles (NPs) show unique magnetic properties depending on their size,[1−4] shape,[5−7] and spatial arrangement.[8−10] Thus, the magnetism of magnetic NPs can be tailored by controlling the size, shape, and arrangement of the particles.[7,9,11−13] Magnetic NPs show great potential in various fields, especially in industrial and bio applications.[14−21] Flexible and dynamic control of their magnetic properties is attracting growing attention. Since the interparticle interactions depend on the distance between neighboring particles,[8,22−24] controlling the aggregation state enables us to develop magnetic NP systems with the desired properties. Therefore, dynamic control of magnetic interactions between magnetic NPs offers a promising strategy for developing smart materials with tunable magnetic properties, such as sensors and data storage devices.

Received: May 1, 2025
Revised: July 18, 2025
Accepted: July 21, 2025

Downloaded via 146.90.21.3 on August 6, 2025 at 10:55:55 (UTC).
See https://pubs.acs.org/sharingguidelines for options on how to legitimately share published articles.

ACS Publications
© XXXX The Authors. Published by American Chemical Society

https://doi.org/10.1021/acsanm.5c02325
ACS Appl. Nano Mater. XXXX, XXX, XXX−XXX

One of the most effective ways to control the interaction between magnetic NPs is to arrange them into regular arrays. To date, a number of studies in that direction have been reported.[25−29] The most common way to form 3D array structures based on inorganic NPs is slow solvent evaporation.[25,27,30] Slow evaporation has been shown to form well-ordered structures such as face-centered cubic (FCC) and body-centered cubic (BCC). However, in most cases, only a limited range of symmetries is obtained. On the other hand, Macfarlane et al. developed polymer-modified iron oxide magnetic NPs by decorating them with complementary binding groups.[26] The resulting NPs formed targeted 3D array structures based on such complementary interparticle binding. Complementary binding groups such as DNA have also been used to create other types of 3D arrays of nonmagnetic NPs.[31−33] This demonstrated that surface modification with functional organic molecules is a good candidate for the effective control of magnetic NP-based structures.

As a next-generation technology, dynamic control of particle 3D arrays is attracting great attention because it should enable real-time regulation of the properties of inorganic NPs. Dynamic control of magnetic properties is expected to be used as an innovative method, where changing the particle morphology cannot deliver the desired properties.

To date, considerable effort has been devoted to the dynamic control of 3D arrays of nonmagnetic inorganic NPs. DNA-mediated assembly enables the formation of well-ordered and controllable NP arrays that respond to changes in the solvent environment.[34,35] While this approach allows the formation and dynamic control of tailored assemblies, it is limited to confined conditions such as in solution. Stimuli-responsive polymers offer another promising strategy, as polymer−NP composites can respond to external stimuli to modulate NP arrangement.[36,37] However, achieving the precise and reproducible ordering of NPs within polymer matrices remains a significant challenge.

Our previous studies demonstrated that hybridization with liquid-crystalline molecules is a promising method to control the arrangement of inorganic NPs.[38,39] Among them, mesogen-modified inorganic NPs show unique thermo- or photo-responsive self-assembling properties,[40−43] allowing them to exhibit dynamic optical properties such as switchable plasmon dichroism.[41,42,44] Hybridization of NPs with liquid-crystalline molecules for dynamic control of material properties is still being intensively studied by different groups, including our own.[45−48] Berti et al. developed organic−inorganic composites, composed of magnetic NPs and lipid liquid crystals for drug delivery systems.[49] The nanocomposites exhibit thermotropic and magnetotropic self-assembled structures that change the particle arrangement from the cubic to hexagonal phase using lipid liquid crystals as scaffolds. The incorporation of NPs into the self-assembled structure of liquid crystals was also shown to be an effective method.

Liquid-crystalline dendrons are good candidates for achieving dynamic control of magnetic NP arrays. In our previous studies, we found that surface modification of inorganic NPs with liquid-crystalline dendrons induces their self-assembly into temperature-responsive ordered structures.[50−52] The chemical structure of the liquid-crystalline dendron molecule used in this work is shown in Figure 1. This structure enables the NPs to self-assemble. Hence, the introduction of these ligands is expected to control the 3D array of magnetic NPs dynamically. In addition, since surface modification with such bulky molecules increases the interparticle distance, the suppression of particle undesirable aggregation is expected, as magnetic attraction is inversely proportional to the sixth power of the interparticle distance. Moreover, our organic−inorganic hybrid dendrimers tend to exhibit irreversible thermal phase transitions.[50,51] This structural irreversibility allows for a clearer investigation of changes in interparticle magnetic interactions before and after structural changes.

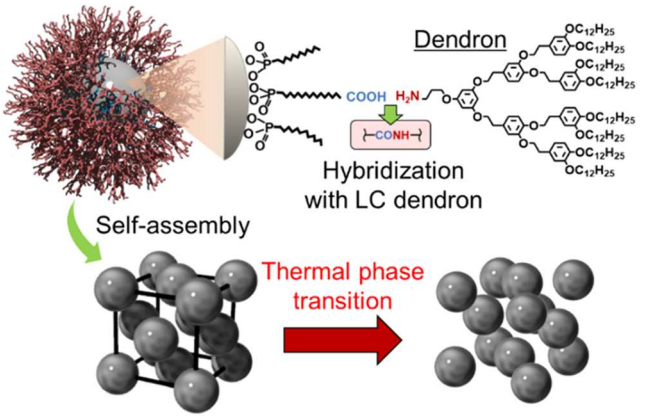

Figure 1. Schematic illustration of dendron-modified FePt NPs.

Based on the above reasons, we have developed dendron-modified magnetic NPs to control the 3D array of magnetic NPs. Iron−platinum (FePt) NPs were selected as the core NPs. FePt NPs with controlled size and shape are easily synthesized,[1,53] and the magnetic properties of FePt NPs can also be significantly affected by interparticle distance.[8,54] Therefore, FePt NPs are regarded as a suitable material for the development of dendrimers with changeable magnetic properties. FePt NPs exhibit both the FCC and $L1_0$ phases, with the latter characterized by high coercivity. However, excessively strong magnetic interactions may disrupt dendrimer self-assembly or lead to undesired aggregation. Therefore, FCC-phase FePt NPs were selected in this study as a model system to demonstrate our concept. In the study of organic−inorganic hybrid materials, surface design is one of the most important points in exhibiting the desired properties. The dendron-FePt NPs were prepared by a two-step surface modification. The first step is to introduce COOH groups onto the surface of FePt NPs via a phosphonic ligand. In this step, the FePt surface coverage by COOH was tuned by dilution with an alkyl coligand. In the second step, dendron modification was carried out by amidation reaction between the COOH and the amino-substituted dendron. In this way, liquid-crystalline organic dendrons were grafted to a controlled degree on the surface of the FePt NPs through chemical bonding. Then, the thermal response of the resulting dendrimer was evaluated by differential scanning calorimetry (DSC) and small-angle X-ray scattering (SAXS). In addition, changes in magnetic properties caused by the array changes were evaluated.

EXPERIMENTAL SECTION

Chemicals. Iron pentacarbonyl ($Fe(CO)_5$) was purchased from Kanto Chemical (Tokyo, Japan). Platinum(II) acetyl acetonate ($Pt(acac)_2$), hexane, ethanol (EtOH), methanol (MeOH), tetrahydrofuran (THF), *N*,*N*-dimethylacetamide, 4-(4,6-dimethoxy-1,3,5-

https://doi.org/10.1021/acsanm.5c02325
ACS Appl. Nano Mater. XXXX, XXX, XXX−XXX

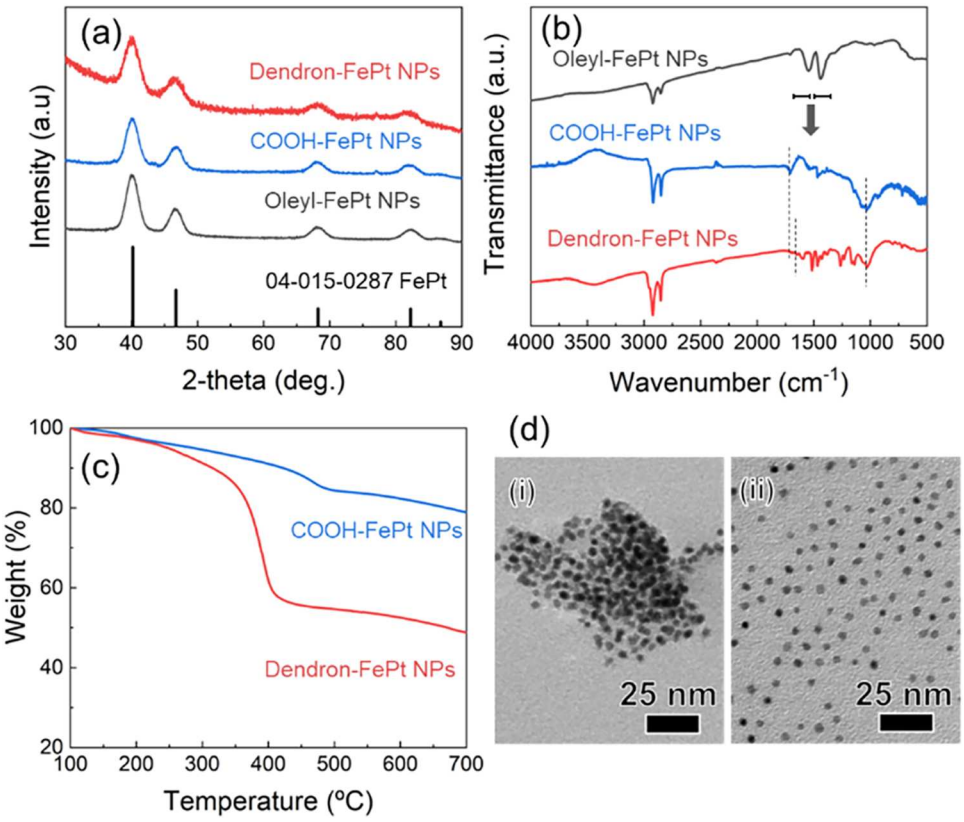

Figure 2. (a) Wide-angle powder X-ray diffractograms and (b) FT-IR spectra of oleyl-FePt NPs, COOH-FePt NPs, and dendron-FePt NPs. The bar graph at the bottom of (a) shows the JCPDS of FePt (No. 04-015-0287). (c) TGA traces of the COOH-FePt NPs and dendron-FePt NPs. (d) TEM images of (i) the COOH-FePt NPs and (ii) the dendron-FePt NPs. The scale bars correspond to 25 nm.

triazin-2-yl)-4-methylmorpholinium chloride (DMT-MM), toluene, and benzene were obtained from FUJIFILM Wako Pure Chemical Corporation (Osaka, Japan).

n-Dodecylphosphonic acid (DPA) and 16-phosphonohexadecanoic acid (PHDA) were provided by Sigma-Aldrich (St. Louis, MO).

The liquid-crystalline dendron was synthesized as previously reported.[50]

Preparation of COOH-FePt NPs. COOH-FePt NPs were prepared through a ligand-exchange reaction using two types of phosphonic acids following our previous report.[55] The experimental procedure was described as the following steps: In the first step, FePt NPs modified with oleylamine and oleic acid were prepared as Nandwana et al. previously reported with minor modification.[1] $Pt(acac)_2$ (0.50 mmol), 0.50 mmol of oleic acid, and 0.50 mmol of oleylamine were mixed and heated to 120 °C under an Ar atmosphere. Then, 1.0 mmol of $Fe(CO)_5$ was injected into the mixture. Afterward, the mixture was heated to 298 °C at a heating rate of 2 °C/min and maintained at the same temperature for 1 h. After cooling to room temperature, the resulting mixture was washed and centrifuged with a Hexane/EtOH mixture (10/30, v/v) 3 times to obtain the oleyl-FePt NPs. In the second step, a ligand-exchange reaction was carried out. One hundred milligrams of oleyl-FePt NPs, 0.32 mmol of DPA, and 0.48 mmol of PHDA were dissolved in a mixture of toluene (15 mL) and *N*,*N*-dimethylacetamide (5 mL). Then, the mixture was stirred at 75 °C for 24 h under an Ar atmosphere. Finally, the resulting mixture was washed with THF/MeOH (10:30) and centrifuged at 18000 rpm for 4 times, and COOH-FePt NPs were obtained.

Preparation of Dendron-FePt NPs. COOH-FePt NPs (20 mg), 200 mg of DMT-MM, and 200 mg of the dendron were dissolved in 4 mL of THF. The mixture was stirred at 60 °C for 24 h under an Ar atmosphere. Then, the resulting mixture was washed with MeOH once, a THF/MeOH mixture (10/30, v/v) 3 times, and a THF/MeOH mixture (15/25, v/v) 2 times successively. Finally, the dendrimer, namely dendron-FePt NPs, was obtained.

Characterization. The crystal structure of the FePt NPs was confirmed by X-ray diffraction (XRD) measurement using a Rigaku Ultima-IV powder diffractometer with a Cu Kα radiation source (40 kV, 40 mA) equipped with a D/teX Ultra detector. The particle morphology and 2D array were observed by transmission electron microscopy (TEM) using a Hitachi H-7650 with an acceleration voltage of 100 kV. Progress of the dendron modification was confirmed by thermal gravimetric analysis (TGA) with a Rigaku Thermo Plus EVO2 and Fourier transform infrared (FT-IR) spectroscopy with SHIMADZU IRAffinity-1S. Nuclear magnetic resonance spectra were measured in a MeOD solution. ^{1}H NMR spectra were recorded on Bruker Avance III 400 at 400 MHz. Chemical shifts (δ, ppm) are reported relative to tetramethylsilane (Me_4Si) as an internal standard (δ = 0.00). Thermal behavior of the resulting dendrimer was evaluated by DSC using Rigaku Thermo plus EVO2 DSCvesta. Phase behavior was also observed by a polarized optical microscope (POM) using a KEYENCE VHX-2000. Structure of the 3D arrays of the resulting FePt-centered dendrimers was investigated by SAXS using a Rigaku Nanoviewer system equipped with a Pilatus detector using a microfocus Cu Kα radiation source (40 kV, 30 mA). For powder SAXS experiments, all samples were prepared by drop-casting a NP dispersion in chloroform onto a Kapton film, followed by drying under ambient conditions. The temperature was controlled with a Mettler FP82 HT hot stage. In addition, grazing incidence SAXS (GISAXS) experiments were performed at SPring-8, beamline BL03XU equipped with a PILATUS 1 M detector (Dectris). The GISAXS sample was prepared on silicon wafer substrates and subjected to benzene vapor annealing at 90 °C for 5 h, followed by cooling to room temperature under a vapor atmosphere to promote the formation of an ordered array. Magnetic properties were determined by a superconducting quantum interference device (SQUID) magnetometer (Quantum Design,

https://doi.org/10.1021/acsanm.5c02325
ACS Appl. Nano Mater. XXXX, XXX, XXX−XXX

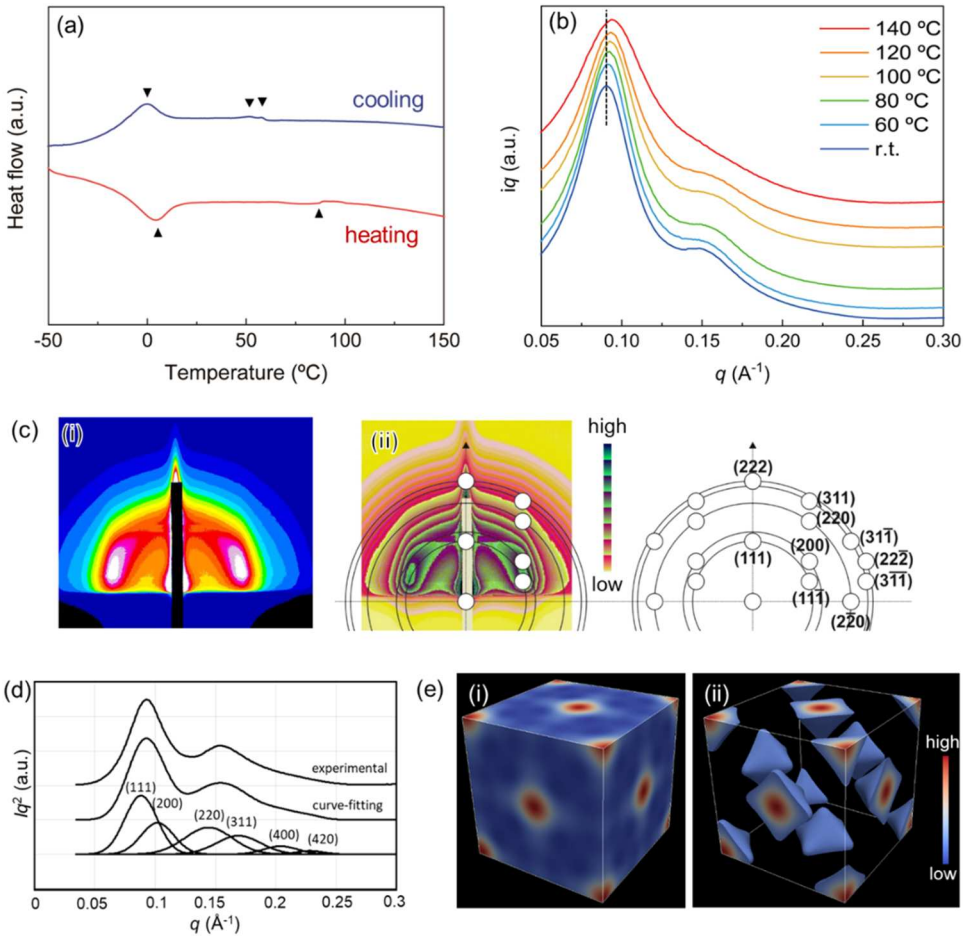

Figure 3. (a) Second heating and cooling DSC thermograms of dendron-FePt NPs. The scanning rate was 10 °C/min. (b) Transmission SAXS traces of dendron-FePt NPs. (c) (i) GISAXS patterns of dendron-FePt NPs recorded at room temperature with vapor annealing. (ii) Calculated positions of Bragg reflections for the FCC phase oriented with its densely packed (111) plane facing the Si substrate, compared with (ii). Color code for (i): blue = low; white = high; the sawtooth color scale for (ii) is shown to the right of the pattern. (d) Result of fitting the 1D SAXS curve of dendron-FePt NPs at room temperature to an FCC lattice with parameter a = 12.3 nm. The top, middle, and bottom graphs show, respectively, the experimental curve, the fitted curve, and the individual Gaussian components. (e) Reconstructed ED map of the FCC structure. (i) False color contours along the surfaces delimiting the unit cell and (ii) isoelectron surfaces surrounding the highest-ED 11% of the unit cell volume, i.e., the NPs.

MPMS-5S) and a vibrating sample magnetometer (VSM) (Quantum Design, PPMS).

RESULTS AND DISCUSSION

Preparation of Dendron-FePt NPs. Figure 2a shows powder X-ray diffractograms of oleyl-FePt NPs, COOH-FePt NPs, and dendron-FePt NPs. The patterns show a face-centered cubic (FCC) crystal structure of FePt in all cases, consistent with JCPDS of FePt (No. 04-015-0287). Note the broadening of the Bragg peaks of the NPs due to their small size. The fact that neither the position nor the width of the peaks changes between the different stages of modification proves that the particle crystal structure remains unaffected through the reactions.

Figure 2b shows the FT-IR spectra of oleyl-FePt, COOH-FePt, and dendron-FePt NPs. The FT-IR spectra of the oleyl-FePt NPs show the symmetric and asymmetric COO− stretching vibration bands in the 1510−1650 and 1360−1470 cm^{-1} regions, respectively, confirming the linkage of oleyl groups to the FePt NP.[56] After the ligand exchange, the peaks disappeared, while a peak corresponding to the Fe−O−P bond appeared at 1070 cm^{-1}, indicating that the oleyl ligands had been successfully exchanged for phosphonic ligands.[55] In addition, the peak derived from C═O appeared at 1710 cm^{-1}, suggesting the introduction of the COOH moieties. At the next stage, the peak derived from C═O shifted to 1645 cm^{-1} due to the formation of the amide bond between COOH and amino-substituted dendrons; at the same time, the Fe−O−P bands were still observed after the dendron modification reaction. These results suggested that the ligand-exchange reaction and dendron modification were successfully performed. ^{1}H NMR spectra of ligands separated after particles were dissolved with acid treatment are shown in Figure S3. It indicates that surface modification with DPA and PHDA was successfully performed because we observed the characteristic peaks of ligands. In addition, it also indicated that almost all oleylamine and oleic acid were replaced because the specific peaks derived from the C═C of oleyl ligands were not found around 5.3 ppm. These IR and NMR results indicate that the ligand exchange was nearly complete, and the residual oleyl ligands are considered to be negligible.

Figure 2c shows the TGA curves of the COOH-FePt NPs and dendron-FePt NPs. They show the weight fraction of organic components to be about 16 and 45%, respectively.

https://doi.org/10.1021/acsanm.5c02325
ACS Appl. Nano Mater. XXXX, XXX, XXX−XXX

According to these TGA results, the modification amount of dendron could be calculated as approximately 110 molecules per particle. In addition, the volume fraction of FePt NPs was also calculated as approximately 9.6% (see SI).

Figure 2d shows TEM images of FePt NPs before and after dendron modification. See also the TEM image of oleyl-modified particles in Figure S1 in the Supporting Information (SI); by comparing these images, we did not find any changes in particle size or shape, and the particle diameter was calculated to be 4.6 ± 0.6 nm. Although the close-packed aggregation was observed in COOH-FePt NPs, a similar aggregation was not observed in dendron-FePt NPs, where the interparticle distance was measured as 7.7 ± 1.1 nm. In addition, dendron-FePt NPs exhibited a tendency to form 2D hexagonal arrays. The fast Fourier transform patterns of the TEM images also showed 6-fold symmetry, indicating that the self-assembling property of the dendron was successfully introduced to the FePt NPs, consistent with our previous studies (Figure S7). Furthermore, the stability of the particle dispersion was drastically improved after dendron modification. The dendron-FePt NPs could remain completely dispersed for more than two months. In contrast, oleyl-FePt NPs or COOH-FePt NPs have already shown aggregation within a few days. Dendron modification is thus able to counter the strong interparticle interactions and effectively suppress aggregation.

Dynamic Control of 3D Array Structure by Thermal Annealing. Figure 3a shows the DSC thermograms of dendron-FePt NPs. The endotherm at 4 °C on heating and at 0 °C on cooling is characteristic of the melting and crystallization of the dodecyl chains on the dendron.[57] In addition, a shallow endothermic peak was observed around 86 °C on heating and a weak exothermic doublet around 55 and 59 °C on cooling. The above results suggest that the peaks were derived from a thermal phase transition. When the sample was sheared between glass slides on a hot bench, it suddenly became fluid at around 90 °C. The melting behavior was also observed in optical micrographs at different temperatures (Figure S8). Our previous study demonstrated that the viscosity decreases sharply at the phase transition temperature, leading to structural changes.[58] The appearance of macroscopic fluidity supports the notion that dendron-FePt NP assemblies undergo thermal phase transitions. On the other hand, no birefringence was observed at any temperature in POM observation, implying that, if any ordered phase had formed in the temperature range covered, it must have been of cubic symmetry.

Subsequently, the 3D array structure was investigated by SAXS. Figure 3b presents the temperature-dependent evolution of the SAXS profiles. The SAXS profile at room temperature shows two broad peaks. In contrast, SAXS patterns of oleyl- and COOH-FePt NPs display only a single broad peak, indicative of an amorphous phase (Figure S5). These findings suggest that the dendron-FePt NPs form periodic structures, and the two peaks observed in SAXS arise from the overlap of several Bragg components. In addition, the SAXS profile showed peak shift and broadening between 80 and 100 °C, with complete melting occurring at 140 °C. This temperature response was consistent with that observed by DSC. Since such temperature-dependent behavior was not observed for oleyl- or COOH-FePt NPs (Figure S5), this suggests that the thermal responsiveness of the dendron ligands has been successfully introduced to the FePt NPs. In this study, the self-assembly behavior differed from previous reports.[50,51] Considering that the ratio between the core NPs and dendrons plays a critical role,[50] this difference is likely attributable to variations in NP size, as the diameters of Au, CdS, and FePt-core NPs were approximately 6.8, 3.9, and 4.6 nm, respectively, due to synthesis constraints. At present, it has not been possible to synthesize Au, CdS, and FePt-core dendrimers with identical sizes, making it difficult to conclusively determine whether the NP size is the dominant factor governing the resulting self-organized structures. Addressing this limitation remains an important challenge for future research. Furthermore, differences in interparticle interactions, including magnetic interactions, are also expected to influence the self-assembly process.[26] On the other hand, as observed in previous studies,[50,51] array structures after phase transition were retained even after cooling, indicating that the structural change was irreversible (Figure S9). Our previous studies also show that organic−inorganic hybrid dendrimers have irreversible arrays, although redispersion in a solvent can restore the original structure.[50,51] It might be due to the weak restorative force of the dendron that might cause such results. From a different point of view, the resulting dendrimer could maintain array structures, even after cooling. It enables investigation of the effects of their array structure on their magnetic properties at low temperatures. These results suggest that dendron-FePt NPs are capable of forming regular structures and controlling their arrangement through thermal phase transitions.

To identify the assembled array structure, GISAXS measurements were conducted. Figure 3c shows the GISAXS pattern of dendron-FePt NPs after exposure to toluene vapor at 90 °C, followed by cooling to room temperature under the same vapor atmosphere to promote the formation of a more ordered array. The azimuthally resolved features characteristic of the FCC lattice are discerned in the patterns in Figure 3c(ii). The GISAXS result confirms that the SAXS pattern is a superposition of poorly resolved Bragg peaks. As shown in Figure 3d, the 1D SAXS curve could be fitted by a series of the following diffraction peaks from an FCC lattice: (111), (200), (220), (311), (400), and (420). The best-fit lattice parameter is a = 12.3 nm, assuming that the peaks are Gaussian in shape. However, due to the broadness of the diffraction peaks, the fitting is not uniquely determined, and alternative fits could potentially describe the data. Fortunately, the GISAXS pattern provides additional structural information that, when combined with the SAXS results, enables a unique assignment of the structure to an FCC lattice, with the (111) plane oriented parallel to the substrate surface. The electron density (ED) map was reconstructed from the best-fit diffraction peaks (Table S1) and is shown in Figure 3e. Figure 3e(i) shows the full ED range contour maps of the bounding faces of a unit cell, while Figure 3e(ii) shows only the high-density regions, i.e., the metal particles. It should be pointed out that the map is entirely dominated by FePt (red), with any ED variation in the organic matrix (blue) having a negligible contribution. The ED map shows the high electron density surrounded by low electron density dendrons. Taking that the particles are spherical with a diameter of 4.6 nm and that there are four NPs in a unit cell of 12.3 nm side, the NP volume fraction should be 11%, which roughly agrees with that calculated from the TGA. The isoelectron surface enclosing the highest-ED 11% of volume, shown in Figure 3e(ii), agrees very well with the size of the NPs. The fact that the ED maxima in Figure

https://doi.org/10.1021/acsanm.5c02325
ACS Appl. Nano Mater. XXXX, XXX, XXX−XXX

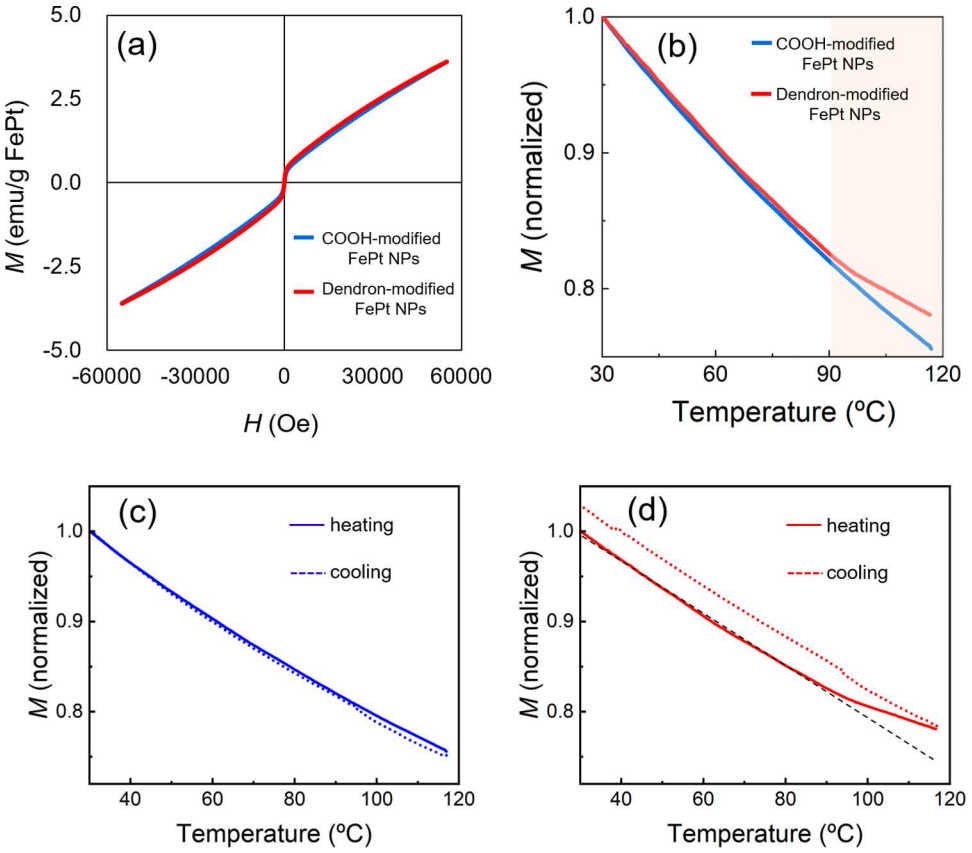

Figure 4. (a) $M-H$ curves of COOH-FePt NPs and dendron-FePt NPs at 300 K in the −5500 to 5500 Oe range. (b) $M-T$ curves of COOH-FePt NPs and dendron-FePt NPs. The samples were annealed in solvent vapor at 90 °C and then inserted into a sample tube. The heating rate was 1 K/min, and measurements were performed every 0.5 K in an inert He atmosphere under a fixed magnetic field of 1000 Oe. $M-T$ curves of (c) the COOH-FePt NPs and (d) dendron-FePt NPs. Solid and dotted lines represent the heating and cooling processes, respectively. The black dashed line in (d) is added as a visual guide to highlight the nonlinear behavior during heating and the linear response during cooling. The same measurement conditions as in (b) were used.

3e(ii) are of octahedral rather than spherical shape can be attributed to the preferential deviation in position along the principal crystallographic axes [100], [010], and [001]. These directions have the lowest compressibility of the dendrons, so collision with the nearest neighbors is the easiest to avoid. The apparent deformation of the spherical shape of the NPs can also be viewed in terms of an anisotropic Debye−Waller factor, which also causes the distortion of the spherical shape of atoms into "ellipsoids of vibration" in 3D representations of crystal structures. It should also be noted that a similar distortion of spherical shape, this time into ellipsoids, has recently been reported in the hexagonal close-packed (HCP) lattice of gold NPs, the distortion being preferentially along the "easy" [0001] direction.[40] These results indicate that dendron-FePt NPs can self-assemble into an FCC phase at room temperature and that their array can be dynamically transformed into an amorphous phase via a thermally induced phase transition.

Changes in Magnetic Properties Through Thermal Annealing. Finally, magnetic properties were investigated during thermal annealing. The magnetic properties of the COOH-FePt NPs and dendron-FePt NPs were compared by VSM and SQUID measurements. Figure 4a shows the corresponding $M-H$ curves. It shows that COOH-FePt NPs and dendron-FePt NPs have similar magnetization. It should be noted that a similar degree of magnetization does not indicate independence from surface dendron modification, as magnetization tends to not only increase with decreasing interparticle distance[23] but also diminish when particles are in extreme proximity.[8] On the other hand, $M-T$ curves of these NPs showed different behavior. Figure 4b shows the $M-T$ curves of the COOH-FePt NPs and dendron-FePt NPs measured from room temperature to 120 °C with a fixed field of 1000 Oe. Due to the common observation in the heating process, the magnetization of COOH-FePt NPs decreased linearly. However, the results of the dendron-FePt NPs showed that the decreasing trend of their magnetization was nonlinear and changed especially around 90 °C. Above 90 °C, the SAXS results show disordered structures and a decrease in interparticle distance, while the $M-T$ curve indicates a trend toward a slower slope of magnetization. Such behavior is not observed in magnetic NPs around room temperature,[59−61] including in single nanosized FePt NPs.[1,62−64] Magnetic NPs have been reported to exhibit an increase in saturation magnetization and a decrease in coercivity even when interparticle distance changes by less than 1 nm.[22,23] In addition, a comparison of the heating and cooling cycles of the $M-H$ curves revealed that the change in magnetic properties of dendron-FePt NPs is irreversible (Figure 4c,b). The magnetization of COOH-FePt NPs showed a linear change during both the heating and cooling processes. In contrast, dendron-FePt NPs exhibited a nonlinear response during heating, while a linear change was observed during cooling. These results indicate that the magnetic property changes induced by the thermal phase transition are

https://doi.org/10.1021/acsanm.5c02325
ACS Appl. Nano Mater. XXXX, XXX, XXX−XXX

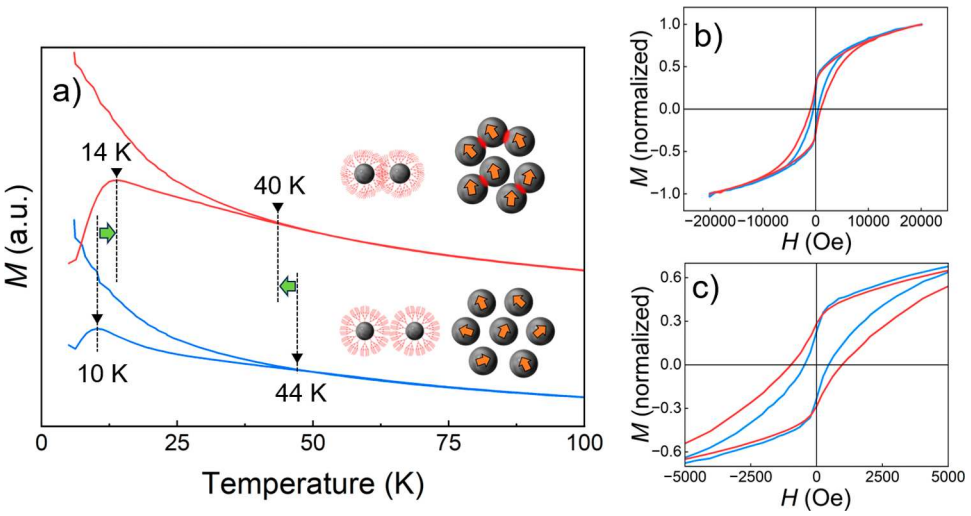

Figure 5. (a) ZFC/FC curves of dendron-FePt NPs before and after annealing at 120 °C. The heating rate was 3 K/min, and measurements were performed every 1 K in an inert He atmosphere under a fixed magnetic field of 50 Oe. (b) $M-H$ curves of dendron-FePt NPs measured at 5K. (c) Enlarged view of (b). Blue and red lines in parts (a−c) represent the data before and after annealing, respectively.

irreversible, consistent with the structural irreversibility observed in the SAXS measurements.

Furthermore, irreversible arrays allow us to compare the interparticle magnetic interactions at low temperatures. Figure 5a shows zero-field-cooled (ZFC)/field-cooled (FC) curves of dendron-FePt NPs before and after annealing at 120 °C. The ZFC curves exhibited a peak corresponding to the blocking temperatures (T_B), which increased from 10 to 14 K after annealing. Since T_B increases with stronger magnetic interaction between adjacent NPs,[22,65] this result suggests that thermal phase transition enhances magnetic coupling due to a reduction in interparticle distance. On the other hand, the temperature at which the ZFC and FC curves deviate decreased after annealing, indicating that magnetic moments begin to freeze at lower temperatures. This behavior is likely attributed to spin frustration caused by increased structural disorder within the array, which promotes the localized freezing of magnetic moments at an earlier stage, consistent with the SAXS results. Figure 5b,c shows $M-H$ curves at 5 K before and after annealing. The result shows an increase in the coercivity, which also supports the enhancement of interparticle magnetic interactions. These findings suggested that the collective magnetic properties are modulated by changes in interparticle magnetic interactions resulting from structural rearrangements. Notably, the comparison of magnetic properties at low temperatures using irreversible array structures provides a deeper insight into the demonstration of our concept of controlling magnetic properties through structural changes. Consequently, these changes in the magnetic properties can be attributed to changes in the 3D arrays.

The above results demonstrate that dendron modification enables us to control their 3D array structures and magnetic properties dynamically. It means that the design of liquid-crystalline molecules on the particle surface enables us to control the changes in their magnetic properties. Hence, the control of the particle array improves the application potential of magnetic NPs used as building blocks for the development of functional materials.

CONCLUSIONS

In this study, liquid-crystalline dendron-FePt NPs were prepared, and their 3D spatial organization was investigated. The resulting FePt NPs showed thermal response in the form of an order−disorder transition due to the introduction of a liquid-crystalline dendron. Structure analysis revealed that the dendron-FePt NPs form the FCC phase, with the lattice parameter changing upon thermal annealing. The results demonstrate that performing surface modification of magnetic NPs with liquid-crystalline dendrons is an efficient way to control the dynamic array structure through thermal stimulus. Furthermore, evaluation of magnetic properties revealed that the thermal phase transition affects the magnetization. It showed that arranging the NPs into a 3D array structure enables their magnetic properties to be controlled dynamically. Hence, the hybridization of magnetic NPs and liquid-crystalline dendrons provides a good bottom-up technology for the development of novel functional magnetic materials. In addition, the structural control of magnetic NPs allowed us to investigate the relationship between magnetic properties and interparticle interaction. This should help in establishing a guide for metamaterials based on magnetic NPs. Therefore, dendron-FePt NPs are also expected to expand the application possibilities of magnetic NPs used as building blocks for functional magnetic materials. These findings suggest that if magnetic properties can be dynamically switched, tuned, or locally controlled in response to various external stimuli, it will pave the way for the development of advanced smart magnetic devices with tunable functionalities, such as sensors and data storage systems.

ASSOCIATED CONTENT

Data Availability Statement

The authors confirm that the data supporting the findings of this study are available within the article and its Supporting Information.

Supporting Information

The Supporting Information is available free of charge at https://pubs.acs.org/doi/10.1021/acsanm.5c02325.

https://doi.org/10.1021/acsanm.5c02325
ACS Appl. Nano Mater. XXXX, XXX, XXX−XXX

STEM image of oleyl-FePt NPs; ^{1}H NMR spectra of PHDA and DPA; ^{1}H NMR spectra of PHDA and DPA recovered from NP surfaces; Schematic diagram for calculating the weight fractions based on TGA data; SAXS results of oleyl- and COOH-FePt NPs; DSC and SAXS results of dendron; TEM image and the corresponding FFT patterns; POM images of dendron-FePt NPs; Indices, calculated scattering vector q-values, and best-fit intensities; and SAXS results of dendron-FePt NPs after cooling (PDF)

AUTHOR INFORMATION

Corresponding Authors

Goran Ungar − *Shaanxi International Research Center of Soft Matter, State Key Laboratory for Mechanical Behavior of Materials, Xi'an Jiaotong University, 710049 Xi'an, China; Department of Materials Science and Engineering, The University of Sheffield, S1 3JD Sheffield, U.K.;* orcid.org/0000-0002-9743-2656; Email: g.ungar@xjtu.edu.cn

Kiyoshi Kanie − *Institute of Multidisciplinary Research for Advanced Materials, Tohoku University, Sendai 980-8577, Japan; International Center for Synchrotron Radiation Innovation Smart, Tohoku University, Sendai 980-8577, Japan;* orcid.org/0000-0003-1477-6515; Email: kanie@tohoku.ac.jp

Authors

Takehiro Yachi − *Institute of Multidisciplinary Research for Advanced Materials, Tohoku University, Sendai 980-8577, Japan;* orcid.org/0000-0001-5301-6231

Rina Sato − *Institute of Multidisciplinary Research for Advanced Materials, Tohoku University, Sendai 980-8577, Japan;* orcid.org/0009-0002-9765-2533

Masaki Matsubara − *Institute of Multidisciplinary Research for Advanced Materials, Tohoku University, Sendai 980-8577, Japan; Department of General Engineering, National Institute of Technology, Sendai College, Natori 981-1239, Japan*

Chen Shen − *Institute of Multidisciplinary Research for Advanced Materials, Tohoku University, Sendai 980-8577, Japan*

Rie Umetsu − *Institute for Material Research, Tohoku University, Sendai 980-8577, Japan*

Xiangbing Zeng − *Shaanxi International Research Center of Soft Matter, State Key Laboratory for Mechanical Behavior of Materials, Xi'an Jiaotong University, 710049 Xi'an, China; Department of Materials Science and Engineering, The University of Sheffield, S1 3JD Sheffield, U.K.;* orcid.org/0000-0003-4896-8080

Atsushi Muramatsu − *Institute of Multidisciplinary Research for Advanced Materials, Tohoku University, Sendai 980-8577, Japan; International Center for Synchrotron Radiation Innovation Smart, Tohoku University, Sendai 980-8577, Japan*

Complete contact information is available at: https://pubs.acs.org/10.1021/acsanm.5c02325

Author Contributions

The manuscript was written through contributions of all authors. All authors have given approval to the final version of the manuscript.

Notes

The authors declare no competing financial interest.

ACKNOWLEDGMENTS

This work was supported by the Japan Society for the Promotion of Science (JSPS) KAKENHI Scientific Research (A) (Grant Numbers JP19H00845 and JP25H00889) to K.K., by JST SPRING (No. JPMJSP2114) and JSPS Fellows (No. JP23KJ0010) to T.Y., by the Natural Science Foundation of China (92156013) to G.U., and by Engineering and Physical Science Research Council (UK) (EP-T003294) to X.Z. This work was performed under the Research Program of "Dynamic Alliance for Open Innovation Bridging Human, Environment and Materials" in "Network Joint Research Center for Materials and Devices" and for the CORE-Lab program. This work was supported by Crossover Alliance to Create the Future with People, Intelligence, and Materials from MEXT, Japan. We also acknowledge Dr. H. Masunaga, Japan Synchrotron Radiation Research Institute, for their SAXS characterization as members of the Frontier Soft Material Beamline (FSBL, BL03XU, Nos. 2021B1733, 2022B7281, 2023A7208, 2024A7207, and 2024B7257) at SPring-8.

ABBREVIATIONS

NPs, nanoparticles; FePt, iron platinum; FCC, face-centered cubic; XRD, X-ray diffraction; TEM, transmission electron microscopy; FT-IR, Fourier transform infrared spectroscopy; DSC, differential scanning calorimetry; SAXS, small-angle X-ray scattering; GISAXS, grazing incidence small-angle X-ray scattering; SQUID, superconducting quantum interference device; VSM, vibrating sample magnetometer; ZFC curve, zero-field-cooled curve; FC curve, field-cooled curve

REFERENCES

(1) Nandwana, V.; Elkins, K. E.; Poudyal, N.; Chaubey, G. S.; Yano, K.; Liu, J. P. Size and Shape Control of Monodisperse FePt Nanoparticles. *J. Phys. Chem. C* **2007**, *111* (11), 4185−4189.

(2) Tong, S.; Quinto, C. A.; Zhang, L.; Mohindra, P.; Bao, G. Size-Dependent Heating of Magnetic Iron Oxide Nanoparticles. *ACS Nano* **2017**, *11* (7), 6808−6816.

(3) Muro-Cruces, J.; Roca, A. G.; López-Ortega, A.; Fantechi, E.; Del-Pozo-Bueno, D.; Estradé, S.; Peiró, F.; Sepúlveda, B.; Pineider, F.; Sangregorio, C.; Nogues, J. Precise Size Control of the Growth of Fe_3O_4 Nanocubes over a Wide Size Range Using a Rationally Designed One-Pot Synthesis. *ACS Nano* **2019**, *13* (7), 7716−7728.

(4) Abdellahi, M.; Tajally, M.; Mirzaee, O. The Effect of the Particle Size on the Heating and Drug Release Potential of the Magnetic Nanoparticles in a Novel Point of View. *J. Magn. Magn. Mater.* **2021**, *530*, No. 167938.

(5) Abenojar, E. C.; Wickramasinghe, S.; Bas-Concepcion, J.; Samia, A. C. S. Structural Effects on the Magnetic Hyperthermia Properties of Iron Oxide Nanoparticles. *Prog. Nat. Sci.* **2016**, *26* (5), 440−448.

(6) Nemati, Z.; Alonso, J.; Rodrigo, I.; Das, R.; Garaio, E.; García, J. Á.; Orue, I.; Phan, M.-H.; Srikanth, H. Improving the Heating Efficiency of Iron Oxide Nanoparticles by Tuning Their Shape and Size. *J. Phys. Chem. C* **2018**, *122* (4), 2367−2381.

(7) Gavilán, H.; Simeonidis, K.; Myrovali, E.; Mazarío, E.; Chubykalo-Fesenko, O.; Chantrell, R.; Balcells, L.; Angelakeris, M.; Morales, M. P.; Serantes, D. How Size, Shape and Assembly of Magnetic Nanoparticles Give Rise to Different Hyperthermia Scenarios. *Nanoscale* **2021**, *13* (37), 15631−15646.

(8) Voggu, R.; Kumar, N.; Rao, C. N. R. Dependence of the Properties of Magnetic Nanoparticles on the Interparticle Separation. *J. Phys. Chem. C* **2008**, *112* (46), 17775−17777.

(9) Gutiérrez, L.; de la Cueva, L.; Moros, M.; Mazarío, E.; de Bernardo, S.; de la Fuente, J. M.; Morales, M. P.; Salas, G. Aggregation Effects on the Magnetic Properties of Iron Oxide Colloids. *Nanotechnology* **2019**, *30* (11), No. 112001.
(10) Mamiya, H.; Furukawa, I.; Cuya Huaman, J. L.; Suzuki, K.; Miyamura, H.; Jeyadevan, B. Evaluation of Interparticle Interactions between Magnetic Nanoparticles Using First Order Reversal Curves and Weiss Temperature. *J. Phys. Commun.* **2021**, *5* (4), No. 045003.
(11) Lisjak, D.; Mertelj, A. Anisotropic Magnetic Nanoparticles: A Review of Their Properties, Syntheses and Potential Applications. *Prog. Mater. Sci.* **2018**, *95*, 286−328.
(12) Li, Z.; Yang, F.; Yin, Y. Smart Materials by Nanoscale Magnetic Assembly. *Adv. Funct. Mater.* **2020**, *30* (2), No. 1903467.
(13) Myrovali, E.; Papadopoulos, K.; Iglesias, I.; Spasova, M.; Farle, M.; Wiedwald, U.; Angelakeris, M. Long-Range Ordering Effects in Magnetic Nanoparticles. *ACS Appl. Mater. Interfaces* **2021**, *13* (18), 21602−21612.
(14) Bauer, L. M.; Situ, S. F.; Griswold, M. A.; Samia, A. C. S. High-Performance Iron Oxide Nanoparticles for Magnetic Particle Imaging - Guided Hyperthermia (HMPI). *Nanoscale* **2016**, *8* (24), 12162−12169.
(15) Wang, X.; Pan, F.; Xiang, Z.; Jia, W.; Lu, W. Magnetic Fe_3O_4@PVP Nanotubes with High Heating Efficiency for MRI-Guided Magnetic Hyperthermia Applications. *Mater. Lett.* **2020**, *262*, No. 127187.
(16) Wang, W.; Tuci, G.; Duong-Viet, C.; Liu, Y.; Rossin, A.; Luconi, L.; Nhut, J.-M.; Nguyen-Dinh, L.; Pham-Huu, C.; Giambastiani, G. Induction Heating: An Enabling Technology for the Heat Management in Catalytic Processes. *ACS Catal.* **2019**, *9* (9), 7921−7935.
(17) Xu, J.; Shang, M.; Ni, X.; Cao, Y. Strategy Based on Rapid Self-Assembly of Magnetic Nanoparticles for Construction of Photonic Crystals. *ACS Appl. Nano Mater.* **2020**, *3* (8), 8052−8059.
(18) Sharifianjazi, F.; Irani, M.; Esmaeilkhanian, A.; Bazli, L.; Asl, M. S.; Jang, H. W.; Kim, S. Y.; Ramakrishna, S.; Shokouhimehr, M.; Varma, R. S. Polymer Incorporated Magnetic Nanoparticles: Applications for Magnetoresponsive Targeted Drug Delivery. *Mater. Sci. Eng., B* **2021**, *272*, No. 115358.
(19) Shen, C.; Oda, Y.; Matsubara, M.; Yabuki, J.; Yamanaka, S.; Abe, H.; Naito, M.; Muramatsu, A.; Kanie, K. Magnetorheological Fluids with Surface-Modified Iron Oxide Magnetic Particles with Controlled Size and Shape. *ACS Appl. Mater. Interfaces* **2021**, *13* (17), 20581−20588.
(20) Shen, C.; Matsubara, M.; Masui, T.; Kishimoto, H.; Yamanaka, S.; Muramatsu, A.; Kanie, K. Magnetorheological Elastomer Films with Controlled Anisotropic Alignment of Polystyrene-Modified Fe_3O_4 Nanoplates. *ACS Appl. Polym. Mater.* **2022**, *4* (10), 7240−7249.
(21) Guo, Q.; Chen, S.; Li, H.; Wang, X.; He, J.; Chu, J.; Guo, J.; Wang, C. Non-Iridescent Magnetite Photonic Crystal Films and Pigments with Enhanced Magnetic Coupling Effect. *Chem. Eng. J.* **2024**, *488*, No. 150969.
(22) Frankamp, B. L.; Boal, A. K.; Tuominen, M. T.; Rotello, V. M. Direct Control of the Magnetic Interaction between Iron Oxide Nanoparticles through Dendrimer-Mediated Self-Assembly. *J. Am. Chem. Soc.* **2005**, *127* (27), 9731−9735.
(23) Wang, D.; Lin, B.; Shen, T.; Wu, J.; Xia, C.; Song, B.; Ai, H. The Effect of Neighbor Distance of Magnetic Nanoparticle Clusters on Magnetic Resonance Relaxation Properties. *Sci. Bull.* **2016**, *61* (13), 1023−1030.
(24) Fleutot, S.; Nealon, G. L.; Pauly, M.; Pichon, B. P.; Leuvrey, C.; Drillon, M.; Gallani, J.-L.; Guillon, D.; Donnio, B.; Begin-Colin, S. Spacing-Dependent Dipolar Interactions in Dendronized Magnetic Iron Oxide Nanoparticle 2D Arrays and Powders. *Nanoscale* **2013**, *5* (4), 1507−1516.
(25) Josten, E.; Wetterskog, E.; Glavic, A.; Boesecke, P.; Feoktystov, A.; Brauweiler-Reuters, E.; Rücker, U.; Salazar-Alvarez, G.; Brückel, T.; Bergström, L. Superlattice Growth and Rearrangement during Evaporation-Induced Nanoparticle Self-Assembly. *Sci. Rep.* **2017**, *7* (1), No. 2802.
(26) Santos, P. J.; Macfarlane, R. J. Reinforcing Supramolecular Bonding with Magnetic Dipole Interactions to Assemble Dynamic Nanoparticle Superlattices. *J. Am. Chem. Soc.* **2020**, *142* (3), 1170−1174.
(27) Brunner, J.; Baburin, I. A.; Sturm, S.; Kvashnina, K.; Rossberg, A.; Pietsch, T.; Andreev, S.; Sturm née Rosseeva, E.; Cölfen, H. Self-Assembled Magnetite Mesocrystalline Films: Toward Structural Evolution from 2D to 3D Superlattices. *Adv. Mater. Interfaces* **2017**, *4* (1), No. 1600431.
(28) Singh, G.; Chan, H.; Baskin, A.; Gelman, E.; Repnin, N.; Král, P.; Klajn, R. Self-Assembly of Magnetite Nanocubes into Helical Superstructures. *Science* **2014**, *345* (6201), 1149−1153.
(29) Mohtasebzadeh, A. R.; Davidson, J. C.; Livesey, K. L.; Crawford, T. M. Tunability and Ordering in 2D Arrays of Magnetic Nanoparticles Assembled via Extreme Field Gradients. *Adv. Mater. Interfaces* **2022**, *9* (26), No. 2201056.
(30) Mohapatra, J.; Elkins, J.; Xing, M.; Guragain, D.; Mishra, S. R.; Liu, J. P. Magnetic-Field-Induced Self-Assembly of $FeCo/CoFe_2O_4$ Core/Shell Nanoparticles with Tunable Collective Magnetic Properties. *Nanoscale* **2021**, *13* (8), 4519−4529.
(31) Jiang, S.; Zhang, F.; Yan, H. Complex Assemblies and Crystals Guided by DNA. *Nat. Mater.* **2020**, *19* (7), 694−700.
(32) Julin, S.; Korpi, A.; Nonappa; Shen, B.; Liljeström, V.; Ikkala, O.; Keller, A.; Linko, V.; Kostiainen, M. A. DNA Origami Directed 3D Nanoparticle Superlattice via Electrostatic Assembly. *Nanoscale* **2019**, *11* (10), 4546−4551.
(33) Sekizawa, Y.; Hasegawa, Y.; Mitomo, H.; Toyokawa, C.; Yonamine, Y.; Ijiro, K. Dynamic Orientation Control of Gold Nanorods in Polymer Brushes by Their Thickness Changes for Plasmon Switching. *Adv. Mater. Interfaces* **2024**, *11* (11), No. 2301066.
(34) Radha, B.; Senesi, A. J.; O'Brien, M. N.; Wang, M. X.; Auyeung, E.; Lee, B.; Mirkin, C. A. Reconstitutable Nanoparticle Superlattices. *Nano Lett.* **2014**, *14* (4), 2162−2167.
(35) Lan, X.; Liu, T.; Wang, Z.; Govorov, A. O.; Yan, H.; Liu, Y. DNA-Guided Plasmonic Helix with Switchable Chirality. *J. Am. Chem. Soc.* **2018**, *140* (37), 11763−11770.
(36) Li, B.; Smilgies, D.-M.; Price, A. D.; Huber, D. L.; Clem, P. G.; Fan, H. Poly(*N*-Isopropylacrylamide) Surfactant-Functionalized Responsive Silver Nanoparticles and Superlattices. *ACS Nano* **2014**, *8* (5), 4799−4804.
(37) Liu, B.; Lu, X.; Qiao, Z.; Song, L.; Cheng, Q.; Zhang, J.; Zhang, A.; Huang, Y.; Chen, T. pH and Temperature Dual-Responsive Plasmonic Switches of Gold Nanoparticle Monolayer Film for Multiple Anticounterfeiting. *Langmuir* **2018**, *34* (43), 13047−13056.
(38) Kanie, K.; Sugimoto, T. Organic-Inorganic Hybrid Liquid Crystals: Hybridization of Calamitic Liquid-Crystalline Amines with Monodispersed Anisotropic TiO2 Nanoparticles. *J. Am. Chem. Soc.* **2003**, *125* (35), 10518−10519.
(39) Kanie, K.; Muramatsu, A. Organic-Inorganic Hybrid Liquid Crystals: Thermotropic Mesophases Formed by Hybridization of Liquid-Crystalline Phosphates and Monodispersed Alpha-Fe2O3 Particles. *J. Am. Chem. Soc.* **2005**, *127* (33), 11578−11579.
(40) Zhao, Y.-Y.; Li, Y.; Cao, Y.; Mehl, G. H.; Liu, F.; Ungar, G. The Effect of Mesogenic Coronas on the Type and Anisotropy of Gold Nanoparticle Superlattices: When Can the Tail Wag the Dog? *Chemistry* **2023**, *29* (11), No. e202203673.
(41) Zhao, Y.-Y.; Cao, Y.; Siligardi, G.; Mehl, G. H.; Liu, F.; Ungar, G. Self-Assembly of Gold Nanoparticles into an Adjustable Plasmonic 3D Lattice Using Janus-Type Forked Mesogenic Ligands. *Chem. - Asian J.* **2022**, *17* (8), No. e202200057.
(42) Cseh, L.; Mang, X.; Zeng, X.; Liu, F.; Mehl, G. H.; Ungar, G.; Siligardi, G. Helically Twisted Chiral Arrays of Gold Nanoparticles Coated with a Cholesterol Mesogen. *J. Am. Chem. Soc.* **2015**, *137* (40), 12736−12739.
(43) Mang, X.; Zeng, X.; Tang, B.; Liu, F.; Ungar, G.; Zhang, R.; Cseh, L.; Mehl, G. H. Control of Anisotropic Self-Assembly of Gold

https://doi.org/10.1021/acsanm.5c02325
ACS Appl. Nano Mater. XXXX, XXX, XXX−XXX

Nanoparticles Coated with Mesogens. *J. Mater. Chem.* **2012**, *22* (22), 11101−11106.
(44) Dintinger, J.; Tang, B.-J.; Zeng, X.; Liu, F.; Kienzler, T.; Mehl, G. H.; Ungar, G.; Rockstuhl, C.; Scharf, T. A Self-Organized Anisotropic Liquid-Crystal Plasmonic Metamaterial. *Adv. Mater.* **2013**, *25* (14), 1999−2004.
(45) Ning, Y.; Yang, S.; Yang, D.-B.; Cai, Y.-Y.; Xu, J.; Li, R.; Zhang, Y.; Kagan, C. R.; Saven, J. G.; Murray, C. B. Dynamic Nanocrystal Superlattices with Thermally Triggerable Lubricating Ligands. *J. Am. Chem. Soc.* **2024**, *146* (6), 3785−3795.
(46) Grzelak, D.; Tupikowska, M.; Vila-Liarte, D.; Beutel, D.; Bagiński, M.; Parzyszek, S.; Góra, M.; Rockstuhl, C.; Liz-Marzán, L. M.; Lewandowski, W. Liquid Crystal Templated Chiral Plasmonic Films with Dynamic Tunability and Moldability. *Adv. Funct. Mater.* **2022**, *32* (16), No. 2111280.
(47) Bhat, S. A.; Rao, D. S. S.; Prasad, S. K.; Yelamaggad, C. V. Chiral Plasmonic Liquid Crystal Gold Nanoparticles: Self-Assembly into a Circular Dichroism Responsive Helical Lamellar Superstructure. *Nanoscale Adv.* **2021**, *3* (8), 2269−2279.
(48) Grzelak, D.; Parzyszek, S.; Moroz, P.; Szustakiewicz, P.; Zamkov, M.; Lewandowski, W. Self-Assembled PbS/CdS Quantum Dot Films with Switchable Symmetry and Emission. *Chem. Mater.* **2019**, *31* (19), 7855−7863.
(49) Mendozza, M.; Montis, C.; Caselli, L.; Wolf, M.; Baglioni, P.; Berti, D. On the Thermotropic and Magnetotropic Phase Behavior of Lipid Liquid Crystals Containing Magnetic Nanoparticles. *Nanoscale* **2018**, *10* (7), 3480−3488.
(50) Kanie, K.; Matsubara, M.; Zeng, X.; Liu, F.; Ungar, G.; Nakamura, H.; Muramatsu, A. Simple Cubic Packing of Gold Nanoparticles through Rational Design of Their Dendrimeric Corona. *J. Am. Chem. Soc.* **2012**, *134* (2), 808−811.
(51) Matsubara, M.; Stevenson, W.; Yabuki, J.; Zeng, X.; Dong, H.; Kojima, K.; Chichibu, S. F.; Tamada, K.; Muramatsu, A.; Ungar, G.; Kanie, K. A Low-Symmetry Cubic Mesophase of Dendronized CdS Nanoparticles and Their Structure-Dependent Photoluminescence. *Chem.* **2017**, *2* (6), 860−876.
(52) Nakajima, H.; Matsuki, D.; Fukunaga, Y.; Toriyama, T.; Shigematsu, K.; Matsubara, M.; Kanie, K.; Muramatsu, A.; Murakami, Y. Self-Assembled Structure of Dendronized CdS Nanoparticles. *Microscopy* **2019**, *68* (4), 342−347.
(53) Nakaya, M.; Tsuchiya, Y.; Ito, K.; Oumi, Y.; Sano, T.; Teranishi, T. Novel Synthesis of FePt Nanoparticles and Magnetic Properties of Their Self-Assembled Superlattices. *Chem. Lett.* **2004**, *33* (2), 130−131.
(54) Srivastava, S.; Samanta, B.; Arumugam, P.; Han, G.; Rotello, V. M. DNA-Mediated Assembly of Iron Platinum (FePt) Nanoparticles. *J. Mater. Chem.* **2007**, *17* (1), 52−55.
(55) Yachi, T.; Matsubara, M.; Shen, C.; Asami, S.; Milbrandt, N. B.; Ju, M.; Wickramasinghe, S.; Samia, A. C. S.; Muramatsu, A.; Kanie, K. Water-Dispersible Fe_3O_4 Nanoparticles Modified with Controlled Numbers of Carboxyl Moieties for Magnetic Induction Heating. *ACS Appl. Nano Mater.* **2021**, *4* (7), 7395−7403.
(56) Lu, Y.; Miller, J. D. Carboxyl Stretching Vibrations of Spontaneously Adsorbed and LB-Transferred Calcium Carboxylates as Determined by FTIR Internal Reflection Spectroscopy. *J. Colloid Interface Sci.* **2002**, *256* (1), 41−52.
(57) Yao, X.; Cseh, L.; Zeng, X.; Xue, M.; Liu, Y.; Ungar, G. Body-Centred Cubic Packing of Spheres - the Ultimate Thermotropic Assembly Mode for Highly Divergent Dendrons. *Nanoscale Horiz* **2017**, *2* (1), 43−49.
(58) Matsubara, M.; Miyazaki, A.; Zeng, X.; Muramatsu, A.; Ungar, G.; Kanie, K. Rheology of Thermotropic Liquid-Crystalline Dendron-Modified Gold Nanoparticles. *Mol. Cryst. Liq. Cryst.* **2015**, *617* (1), 50−57.
(59) Ojha, V. H.; Kant, K. M. Temperature Dependent Magnetic Properties of Superparamagnetic $CoFe_2O_4$ Nanoparticles. *Phys. B* **2019**, *567*, 87−94.
(60) Nadarajah, R.; Tasdemir, L.; Thiel, C.; Salamon, S.; Semisalova, A. S.; Wende, H.; Farle, M.; Barcikowski, S.; Erni, D.; Gökce, B. Formation of Fe-Ni Nanoparticle Strands in Macroscopic Polymer Composites: Experiment and Simulation. *Nanomaterials* **2021**, *11* (8), 2095.
(61) Winiarczyk, K.; Gac, W.; Góral-Kowalczyk, M.; Surowiec, Z. Magnetic Properties of Iron Oxide Nanoparticles with a DMSA-Modified Surface. *Hyperfine Interact.* **2021**, *242* (1), No. 48.
(62) Colak, L.; Hadjipanayis, G. C. Array Formation and Size Effects in Chemically Synthesized FePt Nanoparticles. *J. Appl. Phys.* **2007**, *101* (9), No. 09J108.
(63) Poudyal, N.; Chaubey, G. S.; Rong, C.-B.; Liu, J. P. Shape Control of FePt Nanocrystals. *J. Appl. Phys.* **2009**, *105* (7), No. 07A749.
(64) Slabu, I.; Wiemer, K.; Steitz, J.; Liffmann, R.; Mues, B.; Eisold, S.; Caumanns, T.; Mayer, J.; Kuhl, C. K.; Schmitz-Rode, T.; Simon, U. Size-Tailored Biocompatible FePt Nanoparticles for Dual T_1/T_2 Magnetic Resonance Imaging Contrast Enhancement. *Langmuir* **2019**, *35* (32), 10424−10434.
(65) Sadat, M. E.; Bud'ko, S. L.; Ewing, R. C.; Xu, H.; Pauletti, G. M.; Mast, D. B.; Shi, D. Effect of Dipole Interactions on Blocking Temperature and Relaxation Dynamics of Superparamagnetic Iron-Oxide (Fe_3O_4) Nanoparticle Systems. *Materials* **2023**, *16* (2), 496.

https://doi.org/10.1021/acsanm.5c02325
ACS Appl. Nano Mater. XXXX, XXX, XXX−XXX